Phys. Status Solidi B **252**, No. 5, 1104–1108 (2015) / **DOI** 10.1002/pssb.201451591

physica status solidi b
www.pss-b.com
basic solid state physics

Low defect large area semi-polar (11$\bar{2}$2) GaN grown on patterned (113) silicon

Markus Pristovsek*[,1], Yisong Han[1], Tongtong Zhu[1], Martin Frentrup[1], Menno J. Kappers[1], Colin J. Humphreys[1], Grzegorz Kozlowski[2], Pleun Maaskant[2], and Brian Corbett[2]

[1] Department of Materials Science and Metallurgy, University of Cambridge, 27 Charles Babbage Road, Cambridge CB3 0FS, UK
[2] Tyndall National Institute, Lee Maltings, Dyke Parade, Cork, Ireland

Received 30 September 2014, revised 29 October 2014, accepted 31 October 2014
Published online 9 December 2014

Keywords growth, MOVPE, patterning, semi-polar GaN, silicon, substrates

* Corresponding author: e-mail mp680@cam.ac.uk, Phone: +44 1223 331954, Fax: +44 1223 334537

We report on the growth of semi-polar GaN (11$\bar{2}$2) templates on patterned Si (113) substrates. Trenches were etched in Si (113) using KOH to expose Si {111} sidewalls. Subsequently an AlN layer to prevent meltback etching, an AlGaN layer for stress management, and finally two GaN layers were deposited. Total thicknesses up to 5 µm were realised without cracks in the layer. Transmission electron microscopy showed that most dislocations propagate along [0001] direction and hence can be covered by overgrowth from the next trench. The defect densities were below 10^8 cm^{-2} and stacking fault densities less than 100 cm^{-1}. These numbers are similar to reports on patterned r-plane sapphire. Typical X-ray full width at half maximum (FHWM) were 500" for the asymmetric (00.6) and 450" for the (11.2) reflection. These FHWMs were 50 % broader than reported for patterned r-plane sapphire which is attributed to different defect structures and total thicknesses. The surface roughness shows strong variation on templates. For the final surface roughness the roughness of the sidewalls of the GaN ridges at the time of coalescence are critical.

1 Introduction With its reduced spontaneous and piezoelectric fields, the semi-polar (11$\bar{2}$2) GaN orientation is a promising surface for the fabrication of green and yellow light emitting diodes. The (11$\bar{2}$2) orientation can be obtained by GaN epitaxy on m-plane (1$\bar{1}$00) sapphire substrates. But such layers have a huge density of dislocations in the 10^{10} cm^{-2} range and basal-plane stacking faults (BSFs) in the 10^5 cm^{-1} range [1, 2]. To reduce defects by promoting three dimensional growth several interlayers have been used like ScN [3], CrN [4], InN quantum dot [5], or SiN_x [5, 6] interlayers. Still these do not reduce BSFs below 10^5cm^{-1}. A reduction in BSF was obtained by two step growth with epitaxial lateral overgrowth (ELOG) [7–11]. A related approach of regrowth of patterned nanowires [12, 13] is currently even commercialised.

Very low dislocation densities without any BSFs can be obtained using bulk substrates. Those are cut from 1 to 2 cm thick crystals grown along the [0001] direction. Thus the resulting semi-polar substrates are small and very expensive.

Yet another way to achieve (11$\bar{2}$2) GaN is by epitaxy on patterned (113) Si substrates, first reported in 2008 [14, 15]. When etching (113) Si with KOH, {111} Si facets are exposed. Furthermore, growth of GaN on the (111) Si surface is well established [16]. The (113) and (1$\bar{1}$1) Si planes enclose an angle of 58.5° to each other, which is very similar to the angle of 58.4° between the (11$\bar{2}$2) and (0001) GaN planes. Thus (0001) GaN growing from the trenches will coalesce into a (11$\bar{2}$2) surface. Growth in [0001] direction also avoids the formation of BSFs. A very similar geometry was also realised using patterned r-plane sapphire [17–21]. In this paper we used patterned (113) Si to obtain a (11$\bar{2}$2) GaN templates on a 100 mm diameter wafer.

2 Experimental First homogeneous 35 nm thick SiO_2 and 100 nm thick SiN layers were deposited on 100 mm diameter (113) Si wafers. These layers act as a mask for selective growth and prevent unintentional nucleation of GaN on the (113) Si surface. Next, a regular and uniform pattern of

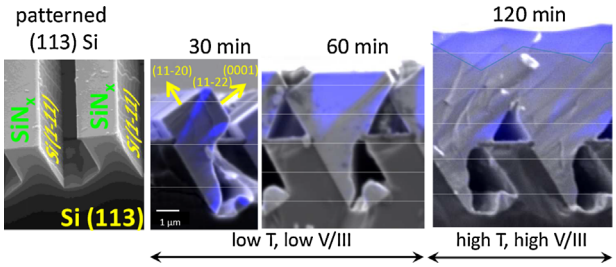

Figure 1 Tilted SEM image of the initial pattern (left) and three cross-section SEM-CL images (pan-chromatic CL signal in blue) during 3D growth and after coalescence.

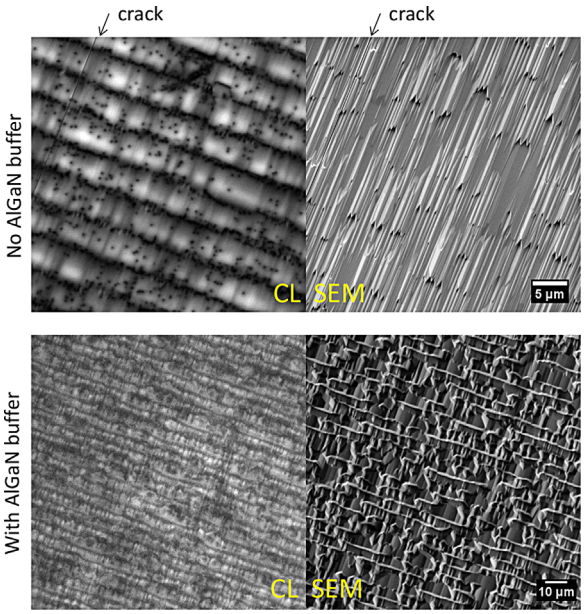

Figure 2 Top view of simultaneously recorded room temperature CL and SEM images of samples without AlGaN buffer layer (top) and with AlGaN buffer (bottom) layer with ≈4 µm GaN thickness. The arrow at the top marks a crack running perpendicular to the trenches. With AlGaN buffer no cracks were observed even on large scale (bottom row). In both samples the density of dark spots is around 5×10^7 cm^{-2}.

trenches parallel to the [21$\bar{1}$] direction was defined into the growth mask by photo-lithography. After oxide/nitride stripping, trenches were etched into the Si surface by immersion in KOH. As a result 2–3 µm deep trenches with exposed {111} facets were obtained. Trench-to-ridge widths of 1:1 µm and 2.5:2.5 µm were studied. An example of a cross-section scanning electron microscope image of patterned (113) Si is shown in Fig. 1 left.

The samples were diced into quarters before loading into the growth reactor. A (113) or (111) Si wafer was co-loaded with a patterned (113) Si sample as a reference structure. This reference wafer also allowed *in situ* optical monitoring of deposition rate and temperature during growth periods in which the specular signal from the (113) Si sample is too small (which is typical for patterned growth).

Growth was performed in a 6×2" close-coupled showerhead metal-organic vapour phase reactor. The initial annealing was at 1065 °C under 40 kPa hydrogen with a total flow of 20 slm for 300–600 s. Then about 10 nm AlN was grown at 1035 °C with 0.22 Pa TMAl, 1000 Pa NH_3 at 10 kPa, followed by 85–100 nm AlN at 1110 °C. On most samples a 400–600 nm $Al_{0.12}Ga_{0.88}N$ buffer layer was deposited at 1020 °C and 465 Pa NH_3 for stress management. Next 3.0–3.5 µm of GaN was grown at 1005 °C at 10–15 kPa and a V/III ratio of 250. Finally 1.5 µm of GaN was grown at 1050 °C with a V/III ratio of 1400 for smoothing the surface. After each run the susceptor was baked at $T > 1200$ °C to remove the residual Ga which would otherwise result in strong meltback etching during Si annealing. Some template were overgrown with a 5× InGaN multi quantum wells (MQWs) to compare the photoluminescence (PL) with similar MQWs on GaN on m-sapphire.

The samples were characterised by optical microscopy, room temperature PL mapping with a 266 nm excitation laser, top view and cross-section cathodoluminescence (CL) at 77 K temperature and room temperature (RT) in a scanning electron microscope (SEM). Dislocation densities were estimated by counting the dark spot density from CL. Using X-ray diffraction (XRD) the full width at half maximum (FHWM) of the (00.6) reflection, (11.2) reflections perpendicular and parallel to [1$\bar{1}$00], and (20.2) reflection were measured. To determine the AlGaN composition we used cross-section CL and XRD measurements of the (20.5) reflection [22]. Finally the BSF density was also estimated using a series of reciprocal space maps (RSMs) from the (20.1) to the (20.5) reflection.

The development of crystal defects in the samples was investigated by transmission electron microscopy (TEM). Cross-sectional TEM thin foils were prepared perpendicular to the trenches (i.e. along the [1$\bar{1}$00] zone axis), and then measured in a Philips CM30 microscope.

3 Results and discussion The GaN layer coalesced quickly when grown on the smaller mask spacing of 1 µm trenches and 1 µm ridges. As a result the layer developed cracks. As soon as cracks appear, the bare Si below the surface is exposed to Ga from the growing surface. This results in meltback which quickly destroys large surface areas. The total GaN thickness was limited to less than 2 µm, which is not sufficient for a good LED structure. Hence most of the experiments focused on the pattern with 2.5 µm wide trenches and 2.5 µm wide ridges.

Without an AlGaN buffer layer the samples developed cracks with a spacing of 50–100 µm which run perpendicular to the trenches (Fig. 2 top row). These cracks originate from the strain from the thermal mismatch between the GaN layer and the Si during cooling down after growth. By inserting an AlGaN buffer between the AlN and GaN the cracking could be avoided (Fig. 2 bottom row). However, if the total thickness was increased above 5–6 µm then cracks are observed parallel to the trenches. These results from the tilting of the trenches due to the thermal expansion mismatch between

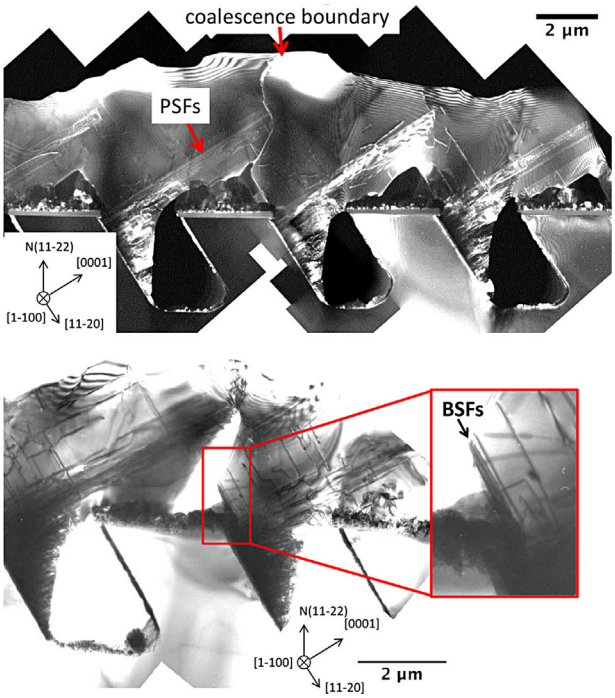

Figure 3 Top shows a cross-sectional weak-beam dark-field TEM image. The planar defects in [0001] direction are likely prismatic stacking faults (PSFs). The coalescence boundary is visible (arrows). Bottom: cross-sectional two-beam bright-field image, showing the existence of BSFs at the (000$\bar{1}$) wings close to the Si substrate.

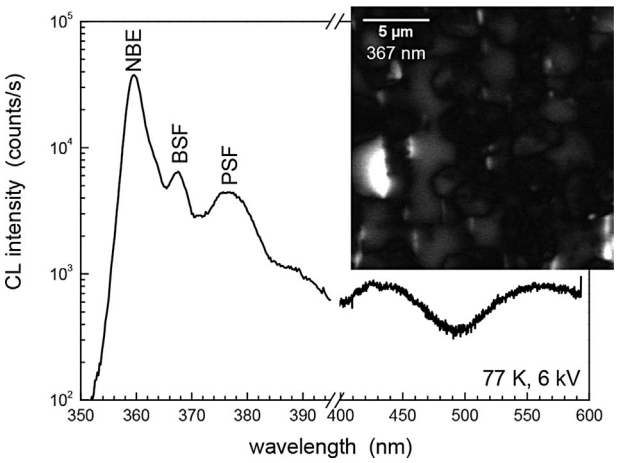

Figure 4 CL spectrum taken at 77 K showing near band edge (NBE), BSF and prismatic stacking fault (PSF) emission. The monochromatic CL image at 367 nm (upper right) shows BSFs as bright signals which a density of 90 cm^{-1}.

GaN and Si when cooling down. Cracks will appear also during growth when the thickness is increased further. Hence the cracking limits the total thickness to about 5–6 µm.

Unlike for planar (111) Si growth which employs several interlayer or grading, only a single AlGaN layer was used with a thickness of about 400–600 nm and (12 ± 1) % Al content. Because the AlGaN nucleates on the whole mask similar to AlN, it can promote the nucleation of unwanted (0001) crystallites perpendicular to the SiN surface. These crystallites grow faster than their neighbouring (11$\bar{2}$2) semi-polar surfaces and will be present on the surface. In order to suppress these parasitic GaN crystallites the AlN and AlGaN layer together must be thin enough and the growth temperature of the AlGaN must be above 1020 °C to reduce nucleation on the mask.

The growth temperature is even more critical for the first GaN layer. As seen in CL cross-section (dark regions in Fig. 1 middle and right) as well as in TEM images (Fig. 3) most dislocations propagate in the [0001] direction which is governed by the growth conditions, i.e. low temperature 3D growth (≈1000 °C). When the temperature and V/III ratio are increased in the final GaN growth step, almost all defects are buried and only few continue at the coalescence border. For comparison when using high temperature 3D growth (e.g. >1100 °C by Tendille et al. [19]) most dislocations propagate perpendicular to [0001]. In the end, both approaches terminate dislocations by lateral overgrowth at (or shortly after) coalescence.

The defect density is reduced by more than one magnitude when using (113) Si in comparison to the best hetero-epitaxial growth on m-sapphire using interlayers. Counting dark spots in CL (Fig. 2) reveals that about 75 % of the dark spots are aligned in the regions where the neighbouring ridges have coalesced. The typical densities of dark spots in CL for growth on patterned (113) Si of $\leq 10^8$ cm^{-2} is similar with earlier results on (113) Si [15] and patterned r-plane sapphire [19, 20]. The QW RT-PL intensities were nearly twice as high as those grown on our best m-sapphire based templates (although the absorbing Si substrate and the roughening due to the pattern make quantitative PL comparison challenging).

The TEM cross-sectional two-beam bright-field image in Fig. 3 (bottom) shows BSFs on the (000$\bar{1}$) wing close above the SiN mask. In CL at 77 K BSFs were identified as I_1 by their luminescence at 367 nm (Fig. 4). They were observed in 5 µm periods in [11$\bar{2}$3] direction which is also the period of the pattern. Comparison with SEM shows that the BSFs occur at the coalescence region of the stripes. The BSFs were on average shorter than 2 µm due to the ragged coalescence region. The BSF density was always <500 cm^{-1} which is similar to reports in literature using patterned substrates [19, 20], and at least a magnitude smaller than what was reported for ELOG [7, 11].

We also tried to determine the BSF density by XRD from the reflection broadening along the *c*-axis as described in Ref. [23] for the (11$\bar{2}$0) orientation and Ref. [24] for the (10$\bar{1}$3) orientation. For our (11$\bar{2}$2) orientation this is much more challenging. Reflections which are sensitive to BSFs, typically (10$\bar{1}l$) and (20$\bar{2}l$), cause a broadening within the {1$\bar{2}$10} zone. However, on (11$\bar{2}$2) orientation this zone cannot be measured in standard skew-symmetric or asymmetric geometry. Therefore, we combined both goniometer

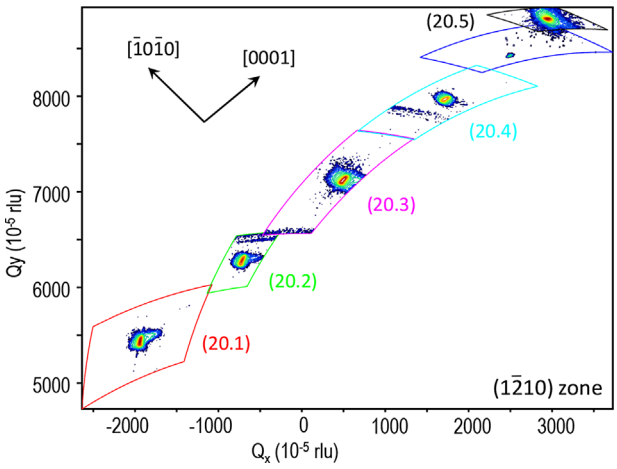

Figure 5 XRD RSMs within the (1$\bar{2}$10) zone show no BSF related streak connecting the (20.*l*) reflections.

geometries to measure a series of reciprocal space maps (RSMs) between the (20.1) and (20.5) reflections. They are shown in Fig. 5. There is no streak visible connecting these reflections which confirms a very low BSF density in our GaN templates.

Figure 6 shows the FHWM of four XRD reflections for growth on patterned (113) Si, for growth on patterned r-plane sapphire [19], and for growth on planar m-sapphire without and with two-step ELOG [8]. Compared to hetero-epitaxial growth on planar m-plane sapphire the FHWM of XRD reflections in Fig. 6 are narrower by a factor of 2. But compared to growth on patterned r-plane sapphire the (11$\bar{2}$2) reflections are still nearly twice as wide despite similar defect densities. The origin is not completely understood. Possible other contributing factors are that layers on r-sapphire are thicker, there might be inhomogeneous strain fields from

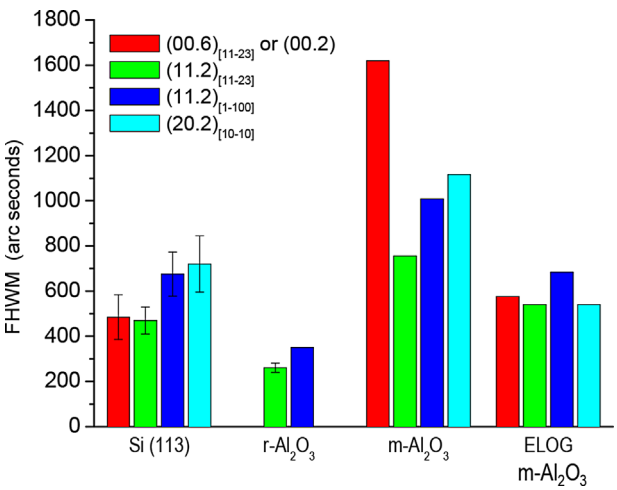

Figure 6 FHWM of four XRD reflections for growth on patterned (113) Si, and from literature on patterned r-sapphire [19], and on planar m-sapphire without and with ELOG [8].

bending of the softer Si due to stress during growth, and there might be different buried defect structures due to the different growth conditions and starting substrates. All (11$\bar{2}$2) layers grown on (113) Si showed no tilt along [11$\bar{2}$3] similar to results on patterned r-plane sapphire.

Recently Okada et al. reported dislocation cluster gliding on m-planes [21]. These showed up as diagonal dark lines in panchromatic CL and an additional broadening after coalescence of (11$\bar{2}$2) RSMs along [11$\bar{2}$3]. Both effects were not observed on our samples. Probably the limited thickness on the Si substrate does not allow to accumulate enough stress to activate this system.

The bow of the semi-polar templates is relatively low because of the brittle 450 μm thick Si (113) substrates. Hence a 100 mm wafer shows a bow below 100 km^{-1}, even though the growth was not optimised for wafer bow yet.

The typical topography of the (11$\bar{2}$2) surface has a higher waviness along [1$\bar{1}$00] and chevron-like features pointing in [11$\bar{2}$3]. These chevrons and the waviness tend to be much larger for patterned growth on r-plane sapphire (e.g. [20]) or ELOG (e.g. [11]). This was also observed on our samples and it is related the growth process. When coalescence occurs then the fast growing (0001) surface touches the slow growing (11$\bar{2}$0) surface. At that point a new (0001) facet collects the atoms on the (11$\bar{2}$0) surface and grows faster than its surrounding. This forms a chevron, since surface diffusion on (11$\bar{2}$2) is faster along [11$\bar{2}$3] than along [1$\bar{1}$00] direction [25].

Hence the smoothness of the (0001) and (11$\bar{2}$0) sidewalls of the ridges can strongly influence the density and size of chevrons and hence the roughness of the final surface. Various degrees of roughness have been observed for a similar growth process on (113) Si templates from different processing runs. Figure 7 (top) shows that the initial topography of the {111} Si sidewalls has many steps and variation in trench depth. On the other hand the GaN at coalescence (Fig. 7 bottom) has many variation in ridge width and height, i.e. a relatively rough (0001) side surface.

As said above, to prevent the formation of chevrons and facets, the sidewalls need to be a smooth as possible. Because etching with KOH is very anisotropic in the [111] Si direction, a small misorientation of the patterns could result in strong variation of step-bunching on the sidewalls and hence a high initial roughness. Intentionally introducing a larger pattern misorientation angle like 2° produced rather pyramidal chains instead of trenches with well-defined step spacing. Therefore we currently investigate the effect of different sample annealing steps and growth conditions on the roughness of the sidewalls.

4 Conclusion We have shown that low defect density, low bow semi-polar (11$\bar{2}$2) GaN templates can be produced on 100 mm diameter patterned (113) Si via growth on the (1$\bar{1}$1) Si sidewalls in etched trenches. To reproducible achieve 5 μm thick coalesced layers we used AlN and AlGaN layers followed by a two-step GaN growth procedure. The growth temperature of the first step is crucial to

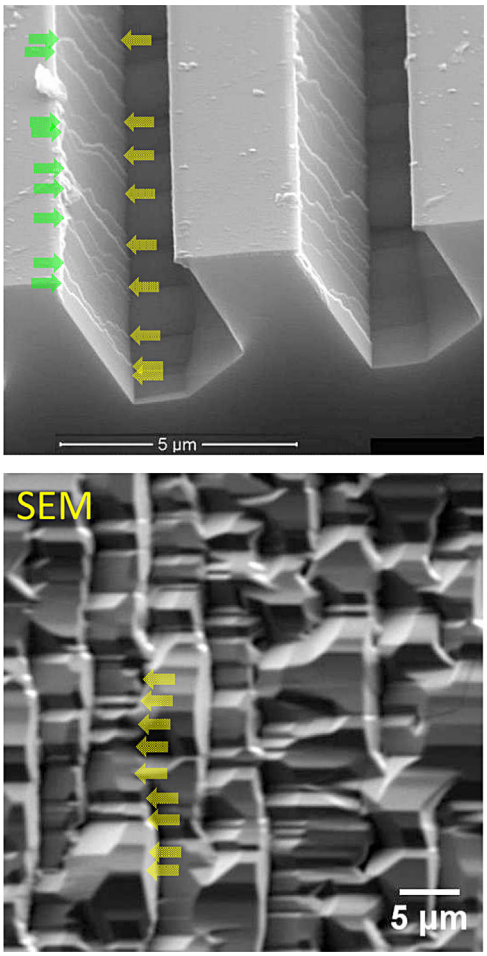

Figure 7 Step bunching on the etched {111} Si and depth modulations on the bottom (top) have similar appearance than the features perpendicular to the trenches on the surface close to GaN coalescence (bottom).

avoid nucleation on the mask and promote propagation of dislocations perpendicular to the fast growing (0001) surface. The remaining challenge is the GaN surface roughness which seems to be connected to roughness of the (0001) and (11$\bar{2}$0) GaN sidewall surfaces at the point of coalescence.

Acknowledgements This work was supported by EU-FP7 ALIGHT No. NMP-2011-280587 and the UK Engineering and Physical Sciences Research Council No. EP/I012591/1.

References

[1] T. J. Baker, B. A. Haskell, F. Wu, J. S. Speck, and S. Nakamura, Jpn. J. Appl. Phys. **45**(2L), L154 (2006).
[2] M. J. Kappers, J. L. Hollander, C. McAleese, C. F. Johnston, R. F. Broom, J. Barnard, M. Vickers, and C. J. Humphreys, J. Cryst. Growth **300**(1), 155 (2007).
[3] C. F. Johnston, M. A. Moram, M. J. Kappers, and C. J. Humphreys, Appl. Phys. Lett. **94**(16), 161109 (2009).
[4] K.-W. Liu, S.-J. Chang, S.-J. Young, T.-H. Hsueh, H. Hung, Y.-C. Mai, S.-M. Wang, and Y.-Z. Chen, J. Electrochem. Soc. **158**(10), H983 (2011).
[5] C. Jung, J. Jang, J. Hwang, J. Jeong, J. Kim, K. Lee, and O. Nam, J. Cryst. Growth **370**, 26 (2013).
[6] M. Ueno, Y. Hashimoto, K. Yamane, N. Okada, and K. Tadatomo, Phys. Status Solidi C **11**(3–4), 557 (2014).
[7] T. Gühne, Z. Bougrioua, P. Vennéguès, M. Leroux, and M. Albrecht, J. Appl. Phys. **101**(11), 113101 (2007).
[8] J. L. Hollander, M. J. Kappers, and C. J. Humphreys, Physica B **401–402**, 307 (2007).
[9] P. de Mierry, N. Kriouche, M. Nemoz, and G. Nataf, Appl. Phys. Lett. **94**(19), 191903 (2009).
[10] T. Zhu, C. F. Johnston, M. J. Kappers, and R. A. Oliver, J. Appl. Phys. **108**(8), 083521 (2010).
[11] T. Zhu, D. Sutherland, T. J. Badcock, R. Hao, M. A. Moram, P. Dawson, M. J. Kappers, and R. A. Oliver, Jpn. J. Appl. Phys. **52**(8S), 08JB01 (2013).
[12] T. Wang, Growth of III-nitride layers for opto-electronic devices using a self-assembled nano-scale mask, UK Patent GB 2488587 A, Seren Photonic Ltd (2012).
[13] K. Xing, Y. Gong, X. Yu, J. Bai, and T. Wang, Jpn. J. Appl. Phys. **52**(8S), 08JC03 (2013).
[14] T. Tanikawa, T. Hikosaka, Y. Honda, M. Yamaguchi, and N. Sawaki, Phys. Status Solidi C **5**(9), 2966 (2008).
[15] T. Tanikawa, Y. Kagohashi, Y. Honda, M. Yamaguchi, and N. Sawaki, J. Cryst. Growth **311**(10), 2879 (2009).
[16] D. Zhu, D. J. Wallis, and C. J. Humphreys, Rep. Prog. Phys. **76**(10), 106501 (2013).
[17] N. Okada, A. Kurisu, K. Murakami, and K. Tadatomo, Appl. Phys. Express **2**(9), 091001 (2009).
[18] B. Leung, Q. Sun, C. Yerino, Y. Zhang, J. Han, B. H. Kong, H. K. Cho, K.-Y. Liao, and Y.-L. Li, J. Cryst. Growth **341**(1), 27 (2012).
[19] F. Tendille, P. D. Mierry, P. Vennégèus, S. Chenot, and M. Teisseire, J. Cryst. Growth **404**, 177 (2014).
[20] F. Scholz, T. Meisch, M. Caliebe, S. Schörner, K. Thonke, L. Kirste, S. Bauer, S. Lazarev, and T. Baumbach, J. Cryst. Growth **405**, 97 (2014).
[21] N. Okada, A. Ishikawa, K. Yamane, K. Tadatomo, U. Jahn, and H. T. Grahn, Phys. Status Solidi A **211**(4), 736 (2014).
[22] D. J. Wallis, D. Zhu, F. Oehler, S. P. Westwater, A. Pujol, and C. J. Humphreys, Semicond. Sci. Technol. **28**(9), 094006 (2013).
[23] M. Barchuk, V. Holý, D. Kriegner, J. Stangl, S. Schwaiger, and F. Scholz, Phys. Rev. B **84**, 094113 (2011).
[24] J. Bläsing, V. Holý, A. Dadgar, P. Veit, J. Christen, S. Ploch, M. Frentrup, T. Wernicke, M. Kneissl, and A. Krost, J. Phys. D **46**(12), 125308 (2013).
[25] S. Ploch, T. Wernicke, D. V. Dinh, M. Pristovsek, and M. Kneissl, J. Appl. Phys. **111**(3), 033526 (2012).

